Diamond & Related Materials 17 (2008) 1998–2004

Contents lists available at ScienceDirect

Diamond & Related Materials

journal homepage: www.elsevier.com/locate/diamond

Micro- and nanomechanical properties of diamond film with various surface morphologies

A. Bogus [a,*], I.C. Gebeshuber [a,b], A. Pauschitz [b], Manish Roy [b], R. Haubner [c]

[a] Institut für Allgemeine Physik, Vienna University of Technology, 1040 Wien, Austria
[b] Austrian Centre of Competence for Tribology, Viktor Kaplan-Strasse 2, 2700 Wiener Neustadt, Austria
[c] Institute of Chemical Technologies and Analytics, Vienna University of Technology, Vienna, Austria

ARTICLE INFO

Article history:
Received 20 February 2008
Received in revised form 21 April 2008
Accepted 18 June 2008
Available online 1 July 2008

Keywords:
Diamond film
Chemical vapour deposition Nanotribology
Morphology

ABSTRACT

The morphologies of chemical vapour deposited (CVD) diamond films can be changed over a wide range by controlling the process parameters of the deposition. The surface morphologies of the film in turn, govern the micro- and nanomechanical properties of the film. In view of these, diamond films having three different types of morphologies namely coarse ballas, fine ballas and faceted, have been deposited using microwave chemical vapour deposition (MWCVD) technique. The morphology, and nature of bonds of these films are characterised with the help of scanning electron microscopy (SEM) and Raman spectroscopy. Hardness of the films is evaluated using nanoindenter. Force spectroscopy, topographies and lateral force values of these films are estimated by means of atomic force microscopy (AFM). Results indicate that films having fine ballas morphology exhibit the minimum roughness whereas film with faceted morphology has highest relative hardness. The friction force was found to be minimum with the film having fine ballas morphology and the friction force was maximum with film having coarse ballas morphology.

1. Introduction

Diamond film is one of the hardest materials and is well known for several extraordinary features such as high mechanical strength [1], excellent thermal conductivity [2], outstanding wear and friction properties [3,4], high chemical inertness [5] etc. These films exhibit high surface roughness because of their columnar growth [6] making it unsuitable for many applications such as in microelectronics and as optical components [7,8]. However, end use tends to favour a particular crystallographic surface texture, purity and thickness matched to the surface that offers the most compatible properties. Thus, properties e.g. broad optical transparency, high refractive index, wide band gap, low or negative electron affinity, transparency to light from deep ultra violet to far infrared and low thermal expansion make these films suitable for numerous industrial applications [9].

Consideration of desired properties of microelectromechanical systems (MEMS) reveals chemical vapour deposited (CVD) diamond as a candidate materials. Development of 'flatland' technology has seen diamond MEMS in the form of seismic mass membrane accelerometer, microspot heater for a liquid ejector [10] and electrostatically actuated microswitch [11]. Amorphous diamond is also used to produce a comb drive actuator [12]. Development of selective deposition micropatterning of diamond on Si and SiO_2 has given movable microgrippers, V-shaped cantilevers and tips for an atomic force microscopy (AFM) [13]. Further, diamond is micromachined by pulsed excimer laser irradiation [14]. Patterning of diamond film by reactive ion eatching has given beam like and turning fork like resonators [15].

Deposition of diamond by CVD process has extensively been studied in the last decade [16,17]. Yugo et al. [18] developed a method to enhance growth rate of diamond by applying a bias enhance nucleation (BEN). This method has also helped in overcoming the difficulties of heteroepitaxial nucleation of diamond on Si substrates with substantial lattice mismatch of 52% between the bulk lattice constant of diamond and Si. Subsequently several studies were conducted employing this method [19–21]. Synthesis of diamond film aims at faceted diamond layers even though hemispherical polycrystalline diamonds (ballases) are also found under non optimal growth conditions [22,23]. The CVD ballas films are also known as cauliflower-like, ball-shaped diamond layers. Faceted diamond layers can be obtained for a wide range of depositing parameter. These methods are based on activation of CH_4/H_2 gas mixtures in order to generate large amounts of atomic hydrogen and carbon radicals [24]. If there is super saturation of carbon in the gas phase, growth conditions of faceted diamond becomes poor and a high density of twins and stacking faults is introduced [25]. This finally, leads to radial growth of polycrystalline unfaceted diamonds of "ballas-type" [26].

In this paper, the influence of surface morphologies such as faceted, fine ballas and coarse ballas on the micro- and nanomechanical properties of microcrystalline diamond film deposited by

* Corresponding author.
E-mail address: bogus@iap.tuwien.ac.at (A. Bogus).

0925-9635/$ – see front matter © 2008 Elsevier B.V. All rights reserved.
doi:10.1016/j.diamond.2008.06.010

Table 1
The important features of the cantilever used for AFM study

Material	Si_3N_4
Cantilever spring constant	0.1 N/m
Cantilever arm length	140 μm
Cantilever arm width	18 μm
Resonance frequency	38 kHz
Full tip opening angle	35°
Tip radius	10 nm

microwave plasma chemical vapour deposition (MWCVD) process has been evaluated.

2. Experimental details

2.1. Deposition of the film

Diamond films were deposited using an ASTEX microwave plasma CVD apparatus. The system has a stainless steel chamber and it operates at 2.45 GHz, 1.5 kW. It is equipped with a heated graphite substrate holder. Silicon (100) substrates scratched with diamond powders were used for deposition of film. Si was scratched with 0.25 mm diamond powders for 30 min and then cleaned ultrasonically. The substrate temperatures were measured with the help of an optical pyrometer. Deposition parameters such as gas pressure, gas flow and microwave power were kept constant. The ratio of CH_4 to H_2, substrate temperature and deposition time were varied.

2.2. Characterisation of the film

The morphologies of the films were examined using a scanning electron microscopy (SEM). Raman spectras were obtained by an integrated confocal microRaman system. LabRam Aramis (Horiba Jobin Yvon) spectrometer equipped with a BXFM confocal microscope and a charge-couple device (CCD) multichannel detector was used for this purpose. The excitation source was a diode pumped solid state (DPSS) laser emitting green light at 532 nm with 50 mW power. On the incoming path, the laser beam was reflected towards the microscope, and the parallel laser beam was then focused onto the sample by a 10× microscope objective. The Raman signal was collected by the same microscope objective and followed the return path to the spectrograph. The backscattered laser light was filtered out. The spectrometer hole and slit widths were set to 1000 μm and 100 μm, respectively and the grating to 1800 grooves/mm.

2.3. AFM measurement

AFM and lateral force microscopy (LFM) images of the films were obtained with an AFM MFP-3D (Asylum Research, Santa Barbara, CA) in air at ambient condition. Silicon nitride tips, triangular cantilevers with a spring constant of 0.1 N m^{-1} were used, the scan area was 5×5 μm^2. Images were recorded in the 'constant-force' mode, that is, feedback electronics and the corresponding software were used to keep the cantilever at constant deflection and to measure the sample topography. In order to obtain the maximum LFM signal (torsion motion), the sample was scanned along the direction perpendicular to the cantilever long axis. The lateral force was evaluated from the difference in the torsional signals (displayed as output voltage) at forward and reverse scans on the lateral force (friction) loop. For each applied force, 512 lateral force loops over a distance of 5 μm were obtained from different regions. The important features of the cantilever used for AFM study are listed in Table 1. Force calibration was performed for each sample.

2.4. Nanohardness measurement

The hardness and the elastic modulus of these films were determined with the help of an instrumented indentation tester equipped with a Berkovich three sided pyramidal diamond indenter

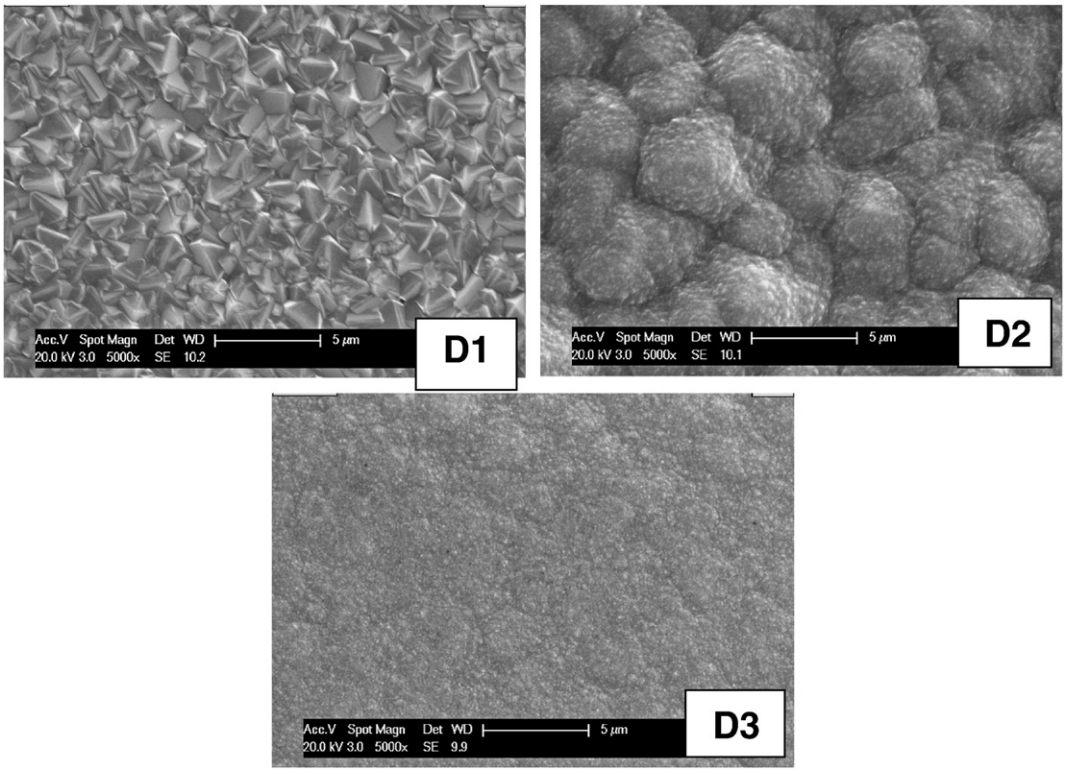

Fig. 1. SEM images showing the morphologies of investigated films.

with a nominal angle equal to 63.5°. The instrument was placed inside a vibration free isolated chamber. This was a depth sensing indenter. The applied load was 4 mN. The load was selected so as to keep the deformation confined within the film. The load and displacement resolution of the instrument was 50 nN and 0.1 nm respectively. The holding time of indentation was 5 s in all cases. Both loading and unloading time was 10 s. The experimental results were corrected for the thermal drift of the equipment, and for the uncertainty in the zero position. The reported hardness and elastic modulus has average of 10 indentations for each sample on different surface position separated by 50 μm. The elastic modulus was determined using a procedure enumerated elsewhere [27]. Elastic modulus was calculated employing Eq. (1) as given below.

$$\frac{1}{E_r} = \frac{(1-\upsilon^2)}{E} + \frac{(1-\upsilon_i^2)}{E_i} \quad (1)$$

and E_r is given by

$$E_r = \frac{0.89S}{\sqrt{A}} \quad (2)$$

Where, S is the slope of the initial part of the unloading curve (in N/m), A is the contact area between the indenter and the substrate (in m^2). E and E_i are the elastic moduli and ν and ν_i are the Poisson ratios of the film and the indenter respectively. The nanoindenter was calibrated by indenting on a fused silica sample and measuring the hardness and elastic modulus of fused silica with hardness and elastic modulus approximately 10 and 73 GPa respectively. Measurement was performed at in a clean air environment with a relative humidity of approximately 40% while the temperature was around 22 °C.

3. Results and discussion

SEM images showing the morphologies of the diamond films are presented in Fig. 1. The morphologies and the structures of the films differ considerably. The film D1 grown at 2% CH_4 consists of crystallites with faceted morphologies having cubo-octahedral and icosahedral symmetries. This crystallite faceted CVD grown diamond can contain many defects [28,29]. Micro twins are mainly observed in (111) growth sectors, while dislocations are mainly observed in the (100) growth sector. Film D2 exhibits radially grown coarse ballas morphology. This morphology is obtained when diamond is grown under condition close to faceted diamond regions [28]. TEM observations of this ballas showed large single crystalline diamond areas in a micro-twined matrix. Film D3 is relatively featureless. In this film also fine ballas can be seen. This ballas morphology can be seen when the film is grown close to graphitic region. This type of morphology is characterised by homogeneous microtwinned matrix.

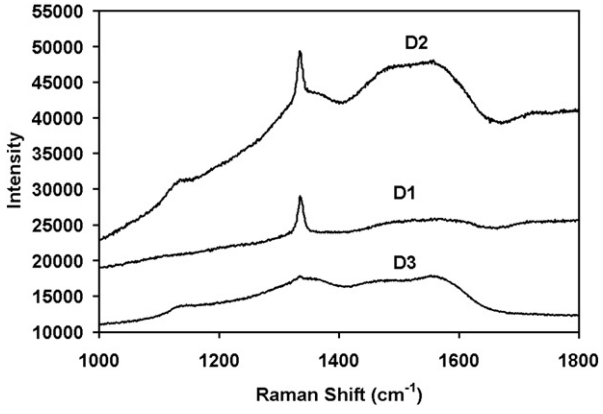

Fig. 2. Raman spectra of investigated films.

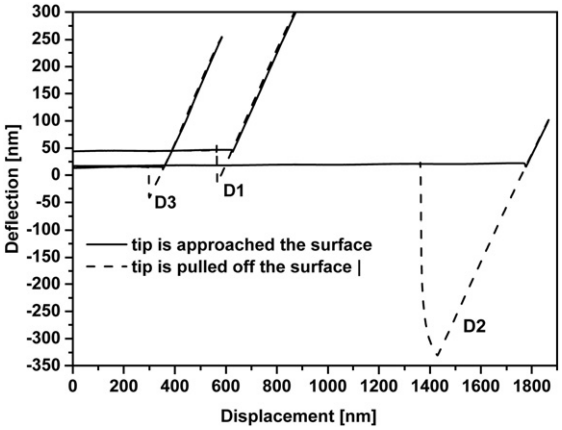

Fig. 3. Force spectroscopy of the investigated films.

Raman spectra obtained from all the films are presented in Fig. 2. All three films show peaks at wave number (1340 cm^{-1}) corresponding to sp^3 bond. The corresponding bond for pure diamond is at 1330 cm^{-1}. This peak is very prominent for the D1 and D2 film and very weak for the D3 film. Film D1 has only one peak. The spectra of the film D2 consist of a broad band between 1400 and 1650 cm^{-1}. This can be deconvoluted in to two peaks at1470 cm^{-1} and 1560 cm^{-1}. The peak at 1470 cm^{-1} is commonly observed in nanocrystalline diamond films [30–33]. Ferrari and Robertson [34] however, assigned this peak to transpolyacetylene situated at the grain boundaries of diamond nanocrystals. The peak at 1560 cm^{-1} can be assigned to the G band of microcrystalline graphite. The presence of this band proves existence of sp^2 bonded carbon within the film. At this point, it should be stated that due to resonance effect [35,36], Raman measurement with excitation at 532 nm is much more sensitive to sp^2 carbon than sp^3 carbon. Film D2 also exhibits the presence of a weak peak at wave number 1160 cm^{-1}. This peak can also be assigned to a diamond nanocrystal. The Raman spectra of the film D3 is characterised by a weak peak at 1160 cm^{-1}, a weak and broad peak in the band of 1300 cm^{-1} to 1400 cm^{-1} and another broad peak in the band from1400 cm^{-1} to 1650 cm^{-1}. These peaks at 1160 cm^{-1} and in the band from 1400 cm^{-1} to 1650 cm^{-1} belong to diamond nanocrystals, G band of microcrystalline graphite and diamond nanocrystal respectively, as described for film D2. The broad peak in the band of 1300 cm^{-1} to 1400 cm^{-1} can be deconvoluted in to two peaks at 1330 cm^{-1} and 1370 cm^{-1}. While the peak at 1330 cm^{-1} corresponds to diamond, the peak at 1370 cm^{-1} will certainly pertain to the D band of microcrystalline graphite. Thus, film D1 is the best diamond film.

To understand the nature of interaction between the cantilever tip and the coating, the deflection displacement curves are recorded. Fig. 3 shows the deflection of the cantilever tip as a function of the distance from the film surfaces for all three films. In all cases, darker line indicates tip approach and lighter line represents the tip being pulled away. The vertical separation between point where the tip is touching the film and point where the tip is pulled off the film is a measure of the pull off (adhesive) force. The product of this horizontal distance of separation and the spring constant of the cantilever (0.1 nN/nm) gives the pull off forces [37]. The pull off forces for film D1, D2 and D3 are 21.3 nN, 81.5 nN and 13.1 nN respectively. It can clearly be seen that the pull off force for film D2 is significantly larger than the pull off forces for film D1 and D3. This fact may be related to increase of surface energy due to oxygen adsorption of the surface. These values are substantially lower than the pull off force calculated to be 445 nN for Ti/*a*-C:H film and comparable to the pull off force of 76.4 nN PECVD diamond film reported previously [38].

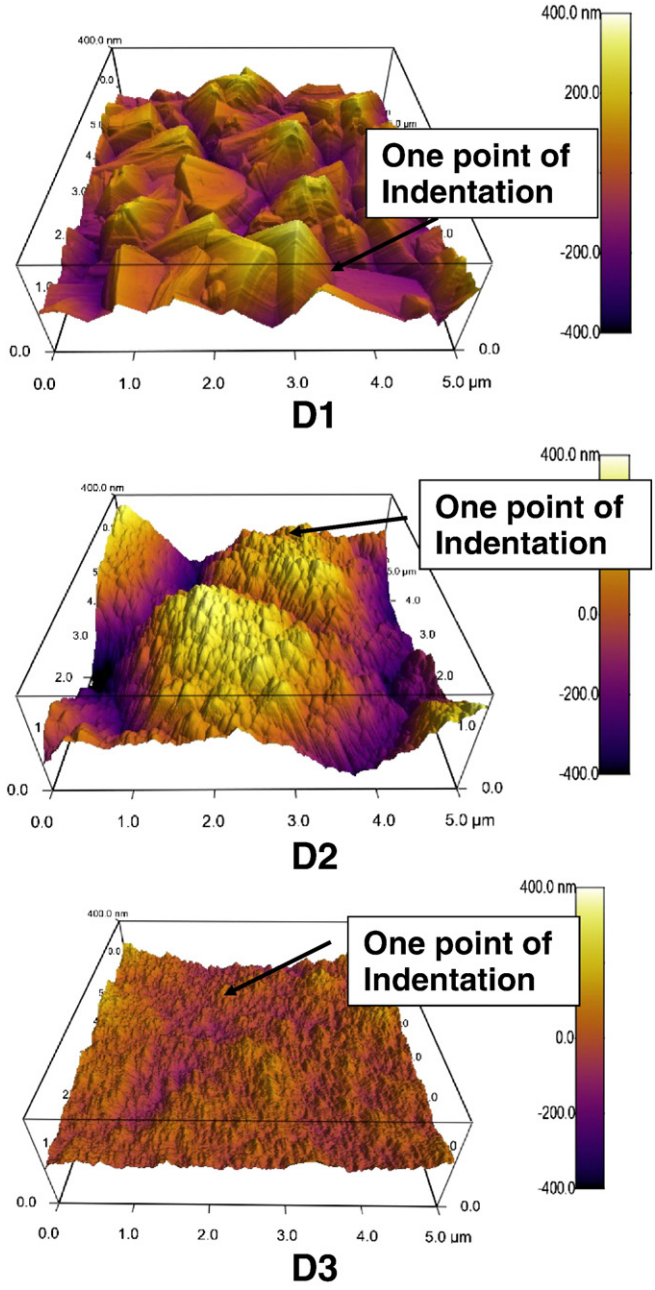

Fig. 4. Topographies of the investigated films.

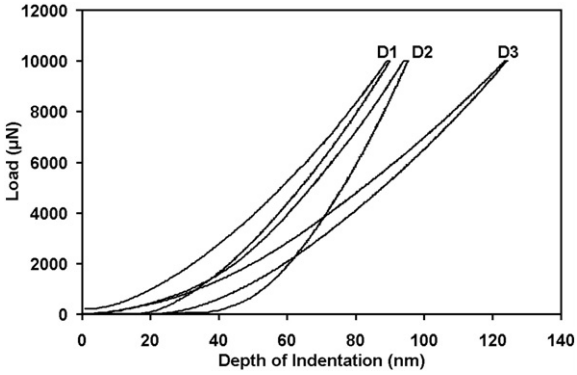

Fig. 5. Load vs. displacement curves of the investigated films.

The three dimensional AFM images showing the topographies of all the films are illustrated in Fig. 4. Film D2 can be characterised with faceted topographical feature. Film D1 exhibits presence of several small peaks on relatively big dome like peak. Film D3 has sharp conical deep but small peaks uniformly distributed. Various topographical parameters are summarised in Table 2. The root mean square (RMS) value of film D2 is higher than that of films D1 and D3. This RMS value is quite high as compared to Ti/*a*-C:H film and PECVD diamond film [38]. However, the maximum height of film D1 and film D3 are comparable with the maximum height of Ti/*a*-C:H film and PECVD diamond film [38].

The load vs. displacement curves for all three films are provided in Fig. 5. The load vs. displacement curves of these films are obtained essentially by superimposition of 10 different curves. It should be mentioned here that the depth of penetration is quite low as compared to the roughness of diamond surfaces. Thus, the roughness criteria is not fulfilled in this case. As higher depth of penetration will result is influence of the substrate, a higher depth of penetration is not possible. However, indentation points are selected carefully. The selected indentation areas for one indentation for each film are marked by arrow in Fig. 4. Given the fact that each curve (load vs. displacement) is super imposition of 10 different curves and given the reproducibility of the data, the load vs. displacement curves can be considered to be at least relative representation of the film properties even though a valid indentation test can not be performed on such rough films. Very high elastic deformation is evident for these films. The maximum depth of penetration and the residual depth of penetration of all these films are summarised in Table 3. The relative elastic modulus and relative hardness of these films are also given in Table 3. The film D3 has the maximum depth of penetration. Film D1 exhibits the minimum depth of penetration and the minimum elastic recovery, as this film has the minimum depth of penetration and the moderate residual depth. The relative elastic modulus of film D1 and D2 are comparable and higher than the elastic modulus of film D3. Among all these films, the maximum relative hardness is exhibited by film D1 having faceted morphology.

Two dimensional AFM images of the friction force values of all three films are displayed in Fig. 6. These images were obtained for an applied load of 4.5 nN and a scan speed of 10 μm s^{-1}. Clearly film D2 has significantly higher friction force than the other two films. The peaks are more prominent in forward scan than in reverse scan, signifying that the friction force on the film is quite high, especially when the film traverses the top of the grain during forward scanning. Furthermore, the average friction force during forward scanning is higher than that during reverse scanning. The friction force of various films are

Table 2
Topographical parameters of the films

Films	Parameters			
	Average height (nm)	R.M.S (nm)	Minimum height (nm)	Maximum height (nm)
D1	−66.0±1.6 9	66.0±1.3	−67.6	−64.3
D2	151.0±9.	151.4±7.8	209.6	152.2
D3	29.9±2.4	30.0±1.7	27.9	33.0

Table 3
Elastic modulus and hardness of various films

Films	Maximum depth of penetration (nm)	Residual depth of penetration (nm)	Elastic modulus (GPa)	Relative hardness (GPa)
D1	90	16	535.5±22.0	82.9±3.4
D2	95	20	563.5±35.0	58.5±4.8
D3	124	20	379.2±38.0	59.3±6.1

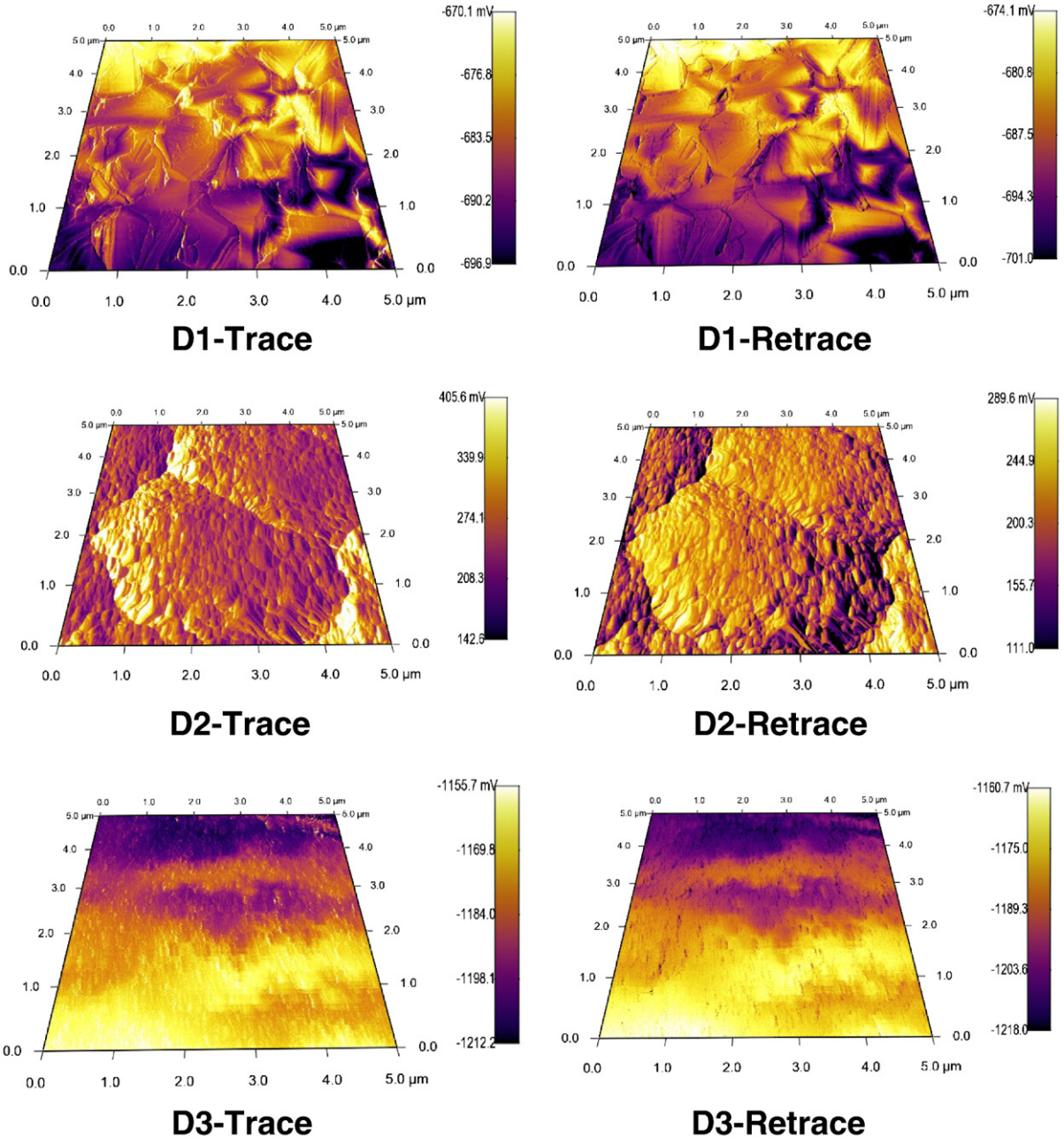

Fig. 6. Lateral force images of the investigated films.

evaluated from the friction force values following the procedure suggested by Beake et al. [39], the friction force (F_L) is given by

$$F_L = 1/2(\mathrm{LF(f)}-LF(\mathrm{r})) \quad (3)$$

where LF(f) and LF(r) are the signals in the forward and reverse direction of motion of the tip in LFM mode. This is based on the fact that when there is substantial variation of the surface topography, the LFM signal contains a component due to normal force acting through the local slope. Since lateral force is determined from the difference between signals reaching the left and the right halves of a four segments photo detector, the topographic contribution of the LFM image may be eliminated by subtracting signals recorded in opposite directions.

The variation of friction force as a function of scan speed for all the films at two different applied loads is presented in Fig. 7. Clearly film D2 has a higher friction force than film D1 and film D3. A higher surface roughness of film D2 compared to films D1 and D3 may be responsible for this behaviour. In general, friction force is independent of scan speed for film D1 and D3. In contrast, friction force decreases with increase of scan speed for film D2. The influence of applied load on the friction force is depicted in Fig. 8. In most of the cases investigated, the friction force decreases with increase of applied load. This suggests that friction force is not governed by ploughing mechanism since in this case, the friction force would increase with increase of applied load when ploughing plays important role. Rather it is controlled by surface force.

Friction can be described as dissipation of energy at the sliding interface. In order to evaluate the possible friction dissipation mechanism, adhesion can be considered to play an important role. Since experiments are conducted in ambient condition the pull off force is a measure of adhesion induced friction force. Perusal of pull off force

and friction force indicates that pull off force increases in the order D3<D1<D2. Similarly the friction force also follows the trend D3<D1<D2. Thus adhesion force influences friction force appreciably.

In the wear under nN load, two additional friction dissipation mechanisms besides adhesion become important. The first mechanism is by emission of photons [40,41]. The second mechanism is energy dissipation by electron-hole pair mechanism [42]. Generally, phononic mechanism is considered to be the dominant mechanism [43,44] in diamond film. In the present investigation, film D1 and D2 are rich in sp^3 hybridisation whereas film D3 is poor in sp^3 hybridisation. Thus, different energy dissipation mechanisms can be considered for these films. If phononic mechanism can be considered to be the dominant mechanism, then the friction force should be either high for both D1 and D2 film and low for D3 film or vice versa. The present observation on friction force indicates completely different behaviour and they are independent of sp^3 hybridisation. Thus in the present work, phononic mechanism does not play influencing role.

It is reported [45] that friction and wear of diamond films can be reduced on the macroscopic scale by adding sp^2 bonds. This observation is valid partially in the present investigation. The friction force is less for D3 having sp^2 bond than film D1 without sp^2 bond. However, the friction force of D2 film having sp^2 bond is higher than the friction force of D1 film. This may possibly be related to the higher roughness of D2 film than D1 film.

At this stage, it should be mentioned that use of microcrystalline films are limited because of their high roughness. In present days, variety of processes are available for depositing nanocrystalline diamond film having low roughness and smooth diamond film [46]. The friction behaviour of nanocrystalline diamond is characterised by roughness independent low friction coefficient and friction coefficient is governed by transfer of carbonaceous film [47]. The wear mechanism in nanocrystalline diamond film is primarily microabrasion [48]. This wear mechanism gives rise to ultra smooth surface and wear coefficient characteristics of mild wear regime [49]. The friction coefficient mostly show high initial friction followed by running in period of low friction coefficient [48]. Unfortunately nanotribology of nanocrystalline diamond film is not yet reported and it appears to be an interesting area of future study. Hitherto no report has been found in relation to transfer of materials in nanotribological study [50]. Thus possibility of carbonaceous transfer layer reducing friction coefficient can be ruled out for the time being. Further, as is the case with most of the materials, nanocrystalline diamond film is expected to have higher hardness than microcrystalline diamond film with similar morphology. However, during nanotribological process, it is the surface force rather than applied load that governs the friction behaviour. Thus increased hardness due to fine grains is unlikely to contribute towards improvement of wear and friction behaviour of nanocrystalline diamond film in nanotribological regime.

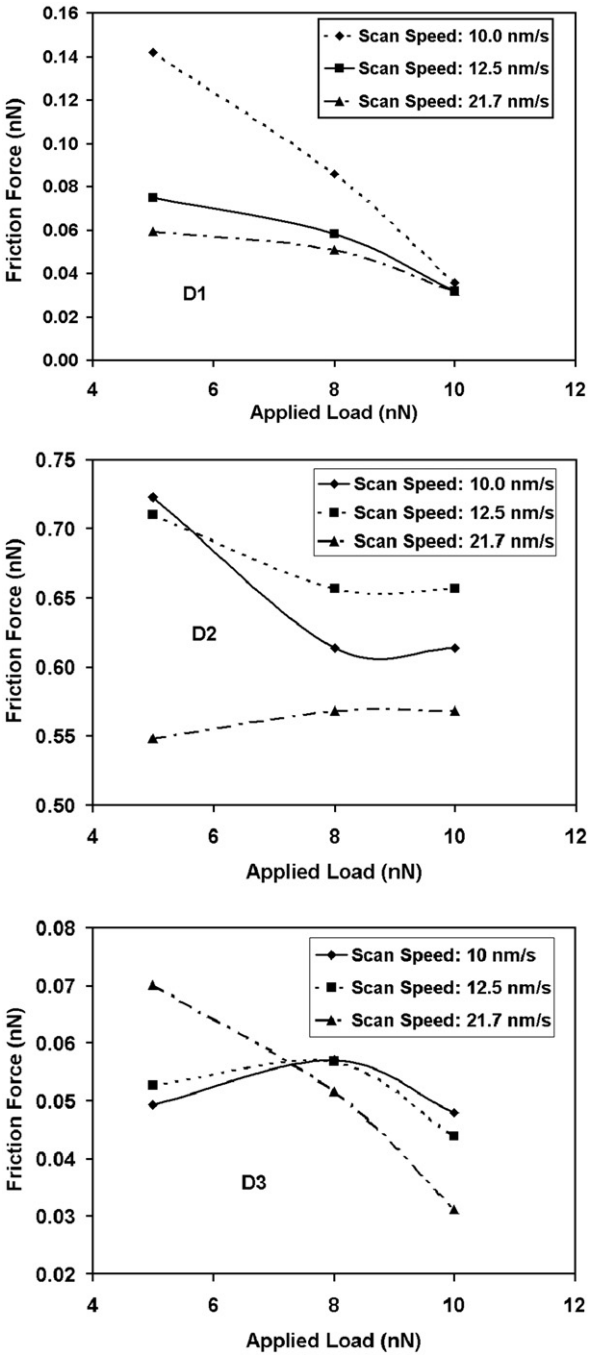

Fig. 8. The influence of applied load on the friction force of the investigated films.

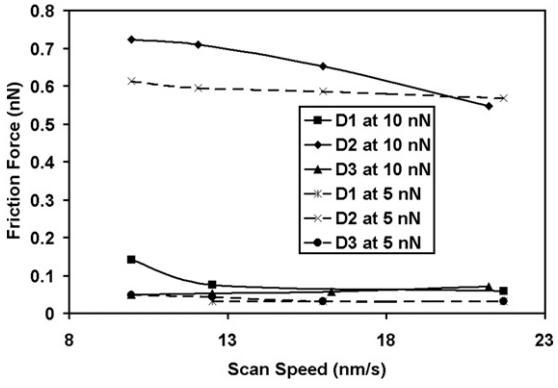

Fig. 7. The influence of scan speed on the friction force of the investigated films.

4. Conclusions

1. The micro and nanomechanical properties of MWCVD diamond films having faceted, fine ballas and coarse ballas morphologies are evaluated.
2. Study with Raman spectroscopy reveals that diamond films with ballas morphologies contain microcrystalline graphite.
3. Diamond film with faceted morphology exhibit highest relative hardness and film having coarse ballas morphology possesses highest relative elastic modulus.

4. The diamond film deposited with faceted morphology gives best combination of morphological, topographical parameters.
5. The friction forces of MWCVD diamond film are governed by adhesion force. The friction force is the minimum with the film having fine ballas morphology.

Acknowledgement

Authors are grateful to European Commission for supporting this work through their programme 'WEMESURF' and through their project No. MIF1-CT-2006-039220. Authors are also grateful to Dr. Thomas Koch from Institute of Materials Science and Technology, Vienna University of Technology, for carrying out the nanoindentation study.

References

[1] K.A. Dean, B.R. Chalamala, Appl. Phys. Lett. 76 (1999) 375.
[2] Diamond Materials and Their Applications, eds. I. Sigals and R.J. Caveney, p. 479.
[3] C. Donnet, Surf. Coat. Technol. 80 (1996) 139.
[4] T. Zehnder, J. Patscheider, Surf. Coat. Technol. 133–134 (2000) 138.
[5] R.L.C. Wu, K. Miyoshi, R. Vuppuladhadium, H.E. Jackson, Surf. Coat. Technol. 54/55 (1992) 576.
[6] R. Haubner, B. Lux, Diamond Rel. Mater, 2 (1993) 1277.
[7] M. Kohzaki, K. Higuchi, S. Noda, K. Uccida, J. Mater. Res. 7 (1992) 1769.
[8] K. Miyoshi, R.L.C. Wu, A. Garscadden, Surf. Coat. Technol. 54/55 (1992) 428.
[9] J. Robertson, Mater. Sci. Eng. R37 (2002) 129.
[10] E. Kohn, P. Gluche, M. Adamschik, Diamond Rel. Mater. 8 (1999) 934.
[11] S. Ertl, M. Adamschik, P. Schmid, P. Gluche, A. Flöter, E. Kohn, Diamond Relat. Mater. 9 (2000) 970.
[12] E. Kohn, M. Adamschik, P. Schmid, S. Ertl, Diamond Rel. Mater. 10 (2001) 1684.
[13] T. Shibata, Y. Kitamoto, K. Unno, E. Makino, J. Microelectromech. Sys. 9 (2000) 47.
[14] J.K. Park, V.M. Ayres, J. Asmussen, K. Mukherjee, Diamond Relat. Mater. 9 (2000) 1154.
[15] I.S. Forbes, J.I.B. Wilson, Thin Solid Films 420–421 (2002) 508.
[16] W.A. Yarbrough, R. Messier, Science 247 (1990) 688.
[17] J.C. Angus, C.C. Hayman, Science 241 (1988) 913.
[18] S. Yugo, T. Kanai, T. Kimura, T. Muto, Appl. Phys. Lett. 58 (1991) 1036.
[19] X. Jiang, C.P. Klages, Diamond Relat. Mater, 2 (1993) 1112.
[20] Y.K. Kim, K.Y. Lee, J.Y. Lee, Appl. Phys. Lett. 68 (1996) 756.
[21] Y.K. Kim, Y.S. Han, J.Y. Lee, Diamond Relat. Mater. 7 (1998) 96.
[22] S. Bühlmann, E. Blank, R. Haubner, B. Lux, Refract. Met. Hard Mater. 20 (2002) 93.
[23] R. Haubner, B. Lux, Diamond Relat. Mater. 9 (2000) 1154.
[24] A. Lindlbauer, Refract. Met. Hard Mater. 11 (1992) 247.
[25] J. Michler, J. Stiegler, Y. von Kaenel, P. Moeckli, W. Dorsch, D. Stenkamp, E. Blank, J. Crystal Growth 172 (1997) 404.
[26] B. Lux, R. Haubner, H. Holzer, R.C. DeVries, Refract. Met. Hard Mater. 15 (1997) 263.
[27] W.C. Oliver, G.M. Pharr, J. Mater. Res. 7 (1992) 1564.
[28] M. Joksh, P. Wurzinger, P. Pongratz, R. Haubner, B. Lux, Diamond Relat. Mater. 3 (1994) 681.
[29] J. Michler, Y. von Kaenel, J. Stiegler, E. Blank, J. Appl. Phys. 83 (1998) 187.
[30] D.M. Gruen, X. Pan, A.R. Krauss, S. Liu, J. Luo, C.M. Foster, J. Vac. Sci. Technol. A 12 (1994) 1491.
[31] R.J. Nemanich, J.T. Glass, G. Lucovsky, R.E. Shroder, J. Vac. Sci. Technol. A6 (1988) 1783.
[32] S. Prawer, K.W. Nugent, D.N. Jamieson, J.O. Orwa, L.A. Bursill, J.L. Peng, Chem. Phys. Lett. 332 (2000) 93.
[33] T. Sharda, M. Umeno, T. Soga, T. Jimbo, J. Appl. Phys. 89 (2001) 4874.
[34] A.C. Ferrai, J. Robertson, Phys. Rev. B. 63 (2001) 121405.
[35] D.S. Night, W.B. White, J. Mater. Res. 4 (1989) 385.
[36] K. Okada, K. Kanda, S. Komatsu, S. Matsumoto, J. Appl. Phys. 88 (2001) 1674.
[37] B. Bhushan, Principles and Applications of Tribology, John Wiley & Sons, New York, USA, 1999 ISBN 0-471-59407-5.
[38] A. Pauschitz, J. Schalko, T. Koch, C. Eissenmenger-Sittner, S. Kvasnica, M. Roy, Bull. Mater. Sci. 26 (2003) 585.
[39] B.D. Beake, I.U. Hassan, C.A. Rego, W. Ahmed, Diamond Relat. Mater. 9 (2000) 1421.
[40] M. Cieplak, E.D. Smith, M.O. Robbins, Science 265 (1994) 1209.
[41] J. Krim, Langmuir 12 (1996) 4564.
[42] B.N.J. Persson, Phys. Rev. B44 (1991) 3277.
[43] P.B. Merrill, S.S. Perry, Surf. Sci. 418 (1998) 342.
[44] S. Kavasnica, J. Schalko, C. Eisenmenger-Sittner, J. Bernardi, G. Vorlaufer, A. Pauschitz, M. Roy, Diamond Relat. Mater. 15 (2006) 1743.
[45] T. Le Huu, M. Schmitt, D. Paulmier, Surf. Sci. 433–435 (1999) 690.
[46] E. Erdemir, G.R. Fenske, A.R. Krauss, D.M. Gruen, T. Macauley, R.T. Csencsits, Surf. Coat. Technol. 120–121 (1999) 565.
[47] R.R. Chromik, A.L. Winfrey, J. Lüning, R.J. Nemanich, K.J. Wahl, Wear 265 (2008) 477.
[48] C.S. Abreu, M. Amaral, A.J.S. Fernandes, F.J. Oliveira, R.F. Silva, J.R. Gomes, Diamond Relat. Mater. 15 (2006) 739.
[49] M. Amaral, C.S. Abreu, A.J.S. Fernandes, F.J. Oliveira, R.F. Silva, J.R. Gomes, Diamond Relat. Mater. 16 (2007) 790.
[50] E. Reido, J. Chevrier, F. Comminand, H. Brune, Surf. Sci. 477 (2001) 25.